ADVANCED OPTICAL MATERIALS
www.advopticalmat.de

Check for updates

Efficient White Light Emission from Ga/Ga_2O_3 Hybrid Nanoparticles

Jin Xiang, Shulei Li, Zhibo Sun, Jingdong Chen, Lei Chen, Mingcheng Pangmai, Guangcan Li, and Sheng Lan**

Gallium (Ga) emerges as a promising material in plasmonics mainly due to its extraordinary properties, such as changeable material phase, tunable plasmon resonances across the ultraviolet to near-infrared spectral range, and remarkable chemical stability. Here, the efficient white light emission from gallium oxide (Ga_2O_3) nanoparticles doped with liquid Ga nanodots, which are fabricated by using a laser-induced oxidation method is reported. The quantum efficiency of Ga/Ga_2O_3 hybrid nanoparticles is found to be ≈1.3%, which is nearly two orders of magnitude larger than that of liquid Ga nanoparticles. It is revealed that the existence of Schottky barrier and hotspots in Ga/Ga_2O_3 nanoparticles plays a crucial role in enhancing the quantum efficiency. As an example of practical applications, high-quality optical data storage is demonstrated by exploiting the controllable formation of Ga/Ga_2O_3 nanoparticles on a platform of disordered Ga nanoislands. These results suggest the potential applications of Ga/Ga_2O_3 hybrid nanoparticles in the development of nanoscale light sources and data storage devices.

1. Introduction

Optical plasmonics has numerous applications in sensing technology, metamaterials, and nonlinear optics, etc.[1–3] Noble metals such as gold (Au) and silver (Ag) have been widely used as plasmon materials due to their excellent optical and thermal properties. Although Ag possesses excellent optical properties, it suffers serious oxidation when exposing to air. Au has outstanding chemical stability, however, the large *d–s* band absorption at high frequencies limits its plasmonic performance in the ultraviolet spectral region.[4] Apart from Ag and Au, gallium (Ga) is now showing great promise because of its unique chemical and physical properties. It has a very low melting point of just 303 K (29 °C) and possesses surface plasmon resonances spanning the ultraviolet to visible spectral region.[5–8] Additionally, Ga is chemically stable because of the existence of a thin gallium oxide (Ga_2O_3) layer on the surface.

Ga nanoparticles (NPs) appear highly promising for surface-enhanced Raman scattering/fluorescence because of their remarkable SPRs.[9–12] The low melting point of Ga renders it an advantage for making all-optical phase-change memory and logic devices,[13] phase transition nonlinear substrates,[14] and high-capacity self-healing anodes in lithium-ion batteries.[15] Recently, it has been experimentally confirmed through real-time ellipsometry the stable coexistence between solid core and liquid shell in substrate-supported Ga NPs.[16] In addition, Ga has excellent flexibility, stretchability, and low toxicity, which makes it an attractive candidate for flexible electronics and wearable sensing devices.[17]

Broadband nanoscale emitters at optical frequencies are now attracting tremendous interest because they are urgently needed for various practical applications, such as ultra-compact optical chips, nanospectroscopy, and active photonic devices.[18,19] Nanoscale white light emitters can be used to probe the near field and to map the local density of states of a nanostructure. However, the achievement of efficient nanoscale white light sources still remains a big challenge. According to Fermi's golden rule,[20,21] the emission intensity of a nanostructure is proportional to the local electric field at the emission wavelength $E_{em}(r, \lambda_{em})$, which is known as the Purcell effect. In addition, it is also closely related to the electric

J. Xiang, S. Li, Z. Sun, M. Pangmai, G. Li, S. Lan
Guangdong Provincial Key Laboratory of Nanophotonic Functional Materials and Devices School of Information and Optoelectronic Science and Engineering
South China Normal University
Guangzhou 510006, P. R. China
E-mail: xiangcos@163.com; slan@scnu.edu.cn

J. Xiang
Key Laboratory of Optoelectronic Technology and Systems (Ministry of Education)
School of Optoelectronic Engineering
Chongqing University
Chongqing 400044, P. R. China

J. Chen
College of Physics and Information Engineering
Minnan Normal University
Zhangzhou 363000, P. R. China

L. Chen
School of Physics and Optoelectronic Engineering
Foshan University
Foshan 528000, P. R. China

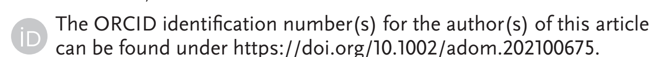
The ORCID identification number(s) for the author(s) of this article can be found under https://doi.org/10.1002/adom.202100675.

DOI: 10.1002/adom.202100675

© 2021 Wiley-VCH GmbH

field at the excitation wavelength $E_{ex}(r, \lambda_{ex})$. There have been several attempts to develop an efficient nanoscale emitter by enhancing either the excitation electric field[22–25] or the emission electric field.[15] For semiconductor emitters, efficient white light emission has been achieved in silicon (Si)[26–28] and gallium arsenide (GaAs)[22] NPs by resonantly exciting their Mie resonances, especially the magnetic dipole (MD) resonance. For metal emitters, white light emission has been observed in Ga NPs[23] and Au hotspots[24,25] by exciting their SPRs. Although nanoscale photon emitters with high quantum efficiencies (>1%) and broadbands (FWHM > 400 nm) are highly desirable for advanced photonic applications, they are not been reported so far.

In this work, we investigated the nonlinear optical responses of Ga NPs placed on a thin Au film. Ga/Ga_2O_3 hybrid NPs fabricated by using laser-induced oxidation were used to realize bright broadband nanoscale photon emitters. Burst of photoluminescence (PL) was observed during the laser-induced oxidation of Ga NPs due to the effective electron transfer at $Ga\text{-}Ga_2O_3$ junction. For practical applications, we demonstrated high-quality optical data storage by using closely-packed Ga nanoislands.

2. Results and Discussion

Ga NPs with diameters (d) ranging from 50 to 300 nm were fabricated using femtosecond laser ablation.[23] Essentially, the PL of a Ga NP is very weak due to the small absorption cross-section even when it is resonantly excited at the electric dipole (ED) resonance. Recently, we proposed a method to improve the excitation efficiency of a Ga NP by placing it on a thin Ag film. It was found that the absorption cross-section can be greatly enhanced at the Fano resonance (or mirror-image-induced MD) formed in the scattering spectrum of the Ga NP. In **Figure 1**a, we show the PL spectra of a Ga NP placed on a thin Au film, which was excited by using femtosecond laser pulses (100 fs and 76 MHz) with different irradiances at 785 nm. Agreeing with our previous observations,[23] we observed broadband emissions at small irradiances by resonantly exciting mirror-image-induced MD (p_x).[29,30] To reveal the optical resonances supported by the Ga NP/Au film, we measured the backward scattering spectrum of the Ga NP. The schematics illustrating the characterization of luminescence and backward scattering of the Ga NP are shown in Figure 1b,c, respectively (see Figure S1, Supporting Information).

To characterize the backward scattering of the Ga NP, a broadband light beam was used to excite the Ga NP and a polarizer was used to control the polarization of the incident light beam. Owing to the existence of the Au film, the SPR of the Ga NP was modified to create a mirror-image-induced MD (p_x mode).[29,30] In addition, a gap mode is excited in the gap between the Ga NP and the Au film.[31,32] Eventually, the coherent interaction between the p_x mode and the g_x mode induces a Fano resonance in the scattering spectrum,[33,34] as shown by the Fano dip in Figure 1d. As shown in Figure 1a, we observed the burst of the PL from the Ga NP when the excitation irradiance exceeded a threshold (≈0.8 mJ cm^{-2}). The PL of the Ga NP after the burst is enhanced by nearly one order

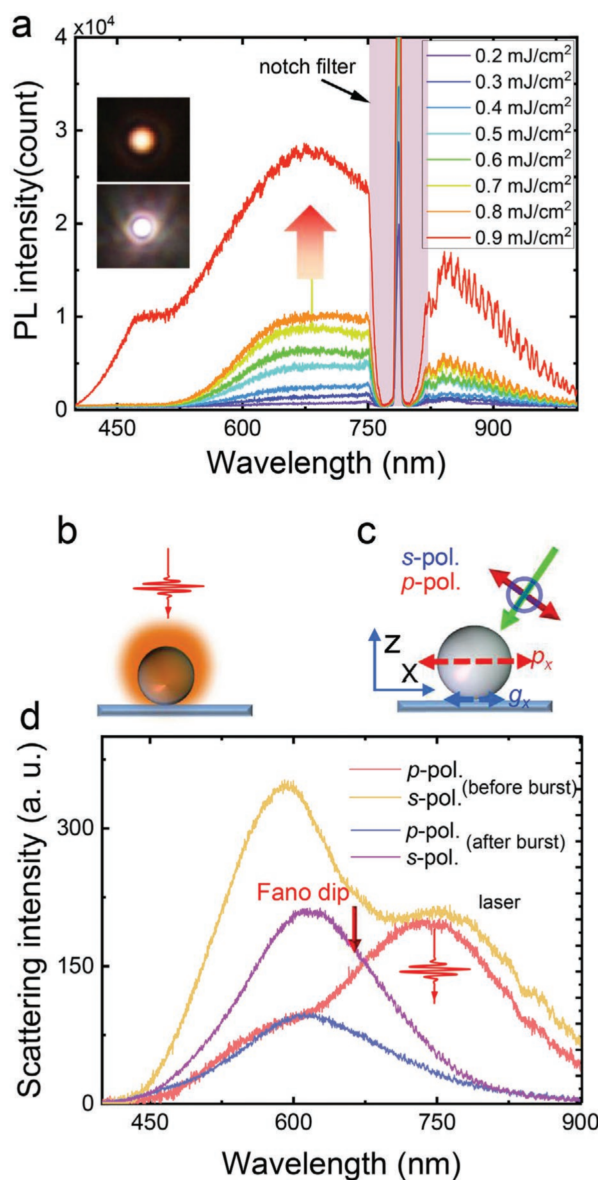

Figure 1. Linear and nonlinear optical responses of Ga NPs. a) PL spectra measured for a Ga NP placed on the Au film at different excitation irradiances. The emission patterns of the Ga NP recorded by using a CCD are shown in the insets. b) Schematic showing the excitation of a Ga NP with femtosecond laser pulses and the PL emitted from the Ga NP. c) Schematic showing the characterization of the backward scattering properties of a Ga NP placed on a thin Au film by using polarized white light. d) Backward scattering spectra measured for a Ga NP with $d \approx 350$ nm before and after the luminescence burst by using white light with polarization angles of 0° (s-polarized) and 90° (p-polarized).

of magnitude and it exhibits very good stability (see Figure S2, Supporting Information). The emission patterns before and after the burst recorded by using a charge-coupled device (CCD) are presented in the insets of Figure 1a. We also examined the morphologies of several Ga NPs before and after the luminescence burst by using scanning electron microscopy (SEM) (see Figures S3 and S4, Supporting Information). It was found that spherical Ga NPs became Ga/Ga_2O_3 NPs with irregular shapes.

 © 2021 Wiley-VCH GmbH

The microscopic mechanisms responsible for the luminescence burst will be discussed in the following.

First, we think that the spherical Ga NP with a liquid core was broken by the high temperature induced by femtosecond laser pulses, generating a large number of Ga NPs with much smaller sizes.[34] These small Ga NPs are randomly distributed in the Ga_2O_3 matrix and closely packed, creating plasmonic hotspots with enhanced electric field. Physically, the extinction of a large NP is dominated by scattering. In contrast, absorption will become dominant in a small NP.[35] The formation of close-packed small Ga NPs will significantly increase the absorption efficiency of the laser light, leading to a rapidly-increased PL.

Second, a spherical Ga NP usually possesses a thin Ga_2O_3 shell that protects the liquid metal core when exposing to air.[5,23,36] Owing to the high temperature induced by femtosecond laser pulses, the self-terminating oxidation of the Ga NP is broken, producing a Ga/Ga_2O_3 hybrid NP. Laser-induced oxidation of metals is a topic of great interest, which can be used for fabricating MOS structures and other semiconductor species.[37–39] In our case, a Ga/Ga_2O_3 hybrid NP possesses metal–semiconductor junctions with a Schottky barrier, which can significantly enhance the PL of the NP.

Liquid metals are devoid of long-range order, so they exist as a "sea" of relatively free electrons coupled to the background of metal ions. In our case, Ga NPs with liquid metal cores behave more like metals with free electrons.[17,40] **Figure 2**a shows the schematic energy band diagram of liquid Ga NPs, which is simplified as a free electron gas model. Since there is no bandgap, high-density hot electrons can be created in the conduction band near the Fermi level through either single- or two-photon-induced absorption. The intraband relaxation of hot electrons can generate an optical emission called hot-electron intraband luminescence.

When two separated materials (i.e., Ga and Ga_2O_3) are brought into contact, a potential energy barrier for electrons, named the Schottky barrier, is formed at the metal–semiconductor (i.e., Ga-Ga_2O_3) junction. The Schottky barrier (W_B) is determined by the vacuum work function of the metal W (4.32 eV for Ga) relative to the vacuum electron affinity E_{EA} (4.0 eV for Ga_2O_3) of the semiconductor, that is, $W_B = W - E_{EA}$. In this case, the equalization of the Fermi levels initiates the movement of electrons from one material to the other. The three-photon-induced absorption of Ga_2O_3 generates hot electrons with energies up to $3h\nu + W_B \approx 5.06$ eV, where $h\nu$ is the energy of the laser photon (1.58 eV) and $W_B \approx 0.32$ eV is the Schottky barrier for the contact between Ga and Ga_2O_3. Essentially, the three-photon-induced absorption in Ga_2O_3 with real states in the valence band is more efficient than the intraband absorption in liquid Ga which needs the assistance of phonons.[18] This difference is responsible for the burst of PL observed in the laser-induced oxidation process (i.e., the formation of Ga/Ga_2O_3 hybrid NPs). Note that the p_x mode is available for enhancing the absorption of the laser light before the luminescence burst and it disappears after the luminescence burst, as shown in Figure 1d.

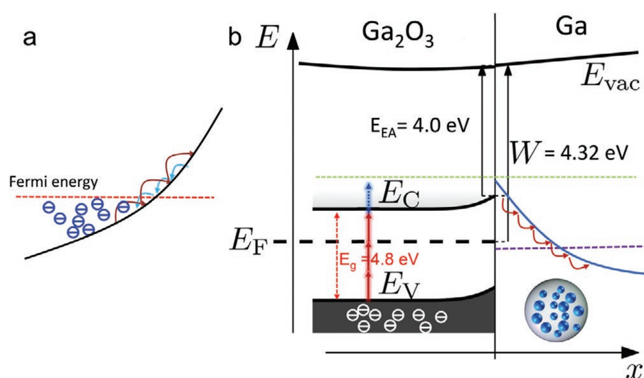

Figure 2. Microscopic mechanisms of the PL from Ga NPs. a) Schematic energy band diagram of liquid Ga NPs, which is considered as a free electron gas. b) Schematic energy band diagram of Ga/Ga_2O_3 NPs.

In order to identify the physical origin for the PL of Ga NPs after the burst, we measured the PL spectra of a Ga/Ga_2O_3 NP at different excitation irradiances, as shown in **Figure 3**a. One can see that the peak of the PL is blueshifted with increasing irradiance, which is quite similar to the blueshift of blackbody radiation with increasing temperature. Eventually, a perfect white light emitter with a bandwidth (FWHM) of ≈400 nm was obtained at an excitation irradiance of 0.18 mJ cm^{-2} (see Figure S5, Supporting Information). Basically, a metallic NP excited by using a femtosecond laser pulse will establish rapidly a Fermi–Dirac distribution that can reach an effective electron temperatures of several thousand degrees Kelvin.[24] The hot-electron intraband luminescence is generally used to describe the PL in this case. It has the significant characteristic that the slope extracted from the PL intensity as a function of the irradiance is linearly proportional to the energy of the emitted photon. To confirm this feature, we plotted the PL intensity of the Ga/Ga_2O_3 NP as a function of the irradiance in a double-logarithmic coordinate, as shown in Figure 3b. Owing to the low electron temperature at small excitation irradiances (0.04–0.06 mJ cm^{-2}), we did not observe the characteristics of hot-electron intraband luminescence. However, it is remarkable that a linear relationship was observed between the slope and the photon energy at large excitation irradiances (0.14–0.18 mJ cm^{-2}), implying that the PL of the Ga/Ga_2O_3 NP is dominated by hot-electron intraband luminescence in this case.

To quantitatively describe the differences between Ga and Ga/Ga_2O_3 NPs as photon emitters, the quantum efficiencies of the PL from these two types of NPs were studied. For Ga/Ga_2O_3 NPs, the unknown multiphoton-induced absorption makes it difficult to estimate the quantum efficiency. Here, we characterized the quantum efficiency of a single NP by exploiting the nonlinear dependence of the multiphoton-induced absorption on the excitation irradiance.[27,28] The experimental setup used to measure the quantum efficiencies of the Ga and Ga/Ga_2O_3 NPs is schematically shown in Note S1, Supporting Information. The key to measuring the multiphoton-induced absorption is that the reflected laser light can be detected in the PL spectra (Figures 1a and 3a), although a stop-band filter with a transmissivity of $\approx 4 \times 10^{-6}$ was used. Since the linear absorption is independent of the excitation irradiance, the intensity of the reflected laser light should be linearly dependent on the excitation irradiance. When the nonlinear absorption becomes significant at high excitation irradiances, a deviation from the linear

 © 2021 Wiley-VCH GmbH

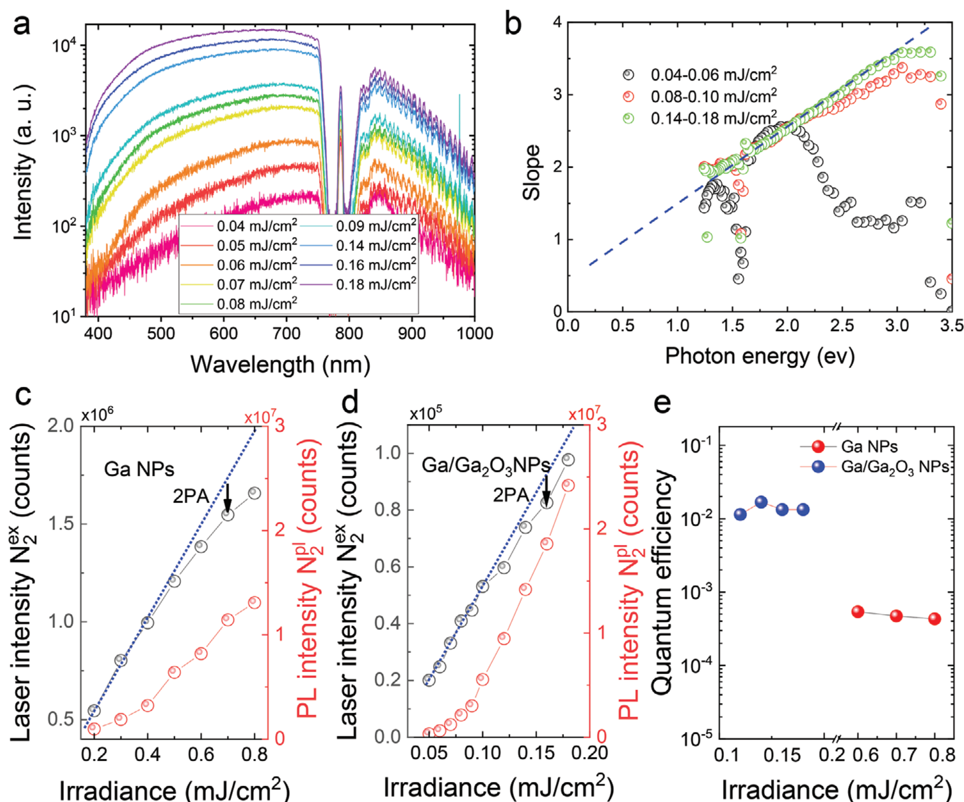

Figure 3. Hot-electron intraband luminescence from Ga and Ga/Ga_2O_3 NPs. a) PL spectra measured for a Ga/Ga_2O_3 NP formed on a thin Au film at different excitation irradiances. The excitation wavelength was chosen to be 785 nm. b) Relationship between the slope extracted from the dependence of the PL intensity on the excitation irradiance and the energy of the emitted photon. c,d) Dependences of the integrated intensities of the PL and the reflected laser light on the excitation irradiances measured for Ga (c) and Ga/Ga_2O_3 NPs (d). The blue dashed line indicates the linear relationship between the intensity of the reflected laser light and the excitation irradiation when the nonlinear absorption is negligible. e) The quantum efficiencies of the Ga and Ga/Ga_2O_3 NPs measured at different irradiances.

relationship was observed. Therefore, we could derive the nonlinear absorption of a NP at high excitation irradiances by using this feature. The equation used for calculating the quantum efficiency can be expressed as follows:

$$Q = N_1^{pl}/N_1^{abs} = N_2^{pl} \times r \times OD \times \eta_{ex} \left(N_2^{abs} \times \beta \times \eta_{pl}\right) \quad (1)$$

Here, N_1^{abs} is the total number of photons absorbed by the NP and N_2^{abs} is the reduced number of photons observed in the reflected light, N_1^{pl} is the number of photons emitted from NP and N_2^{pl} is the number of photons detected by the CCD, η_{ex} is the quantum efficiency of the CCD, r is the reflectivity of the Au film (≈50 nm), OD is the transmissivity of the stop-band filter, β is the collection efficiency of the objective lens (Note S1, Supporting Information, for the detailed derivation).

In Figure 3c,d, we show the dependences of the integrated PL intensity (N_2^{pl}) and reflected laser light intensity (N_2^{ex}) on the excitation irradiance before (Ga NP) and after (Ga/Ga_2O_3 NP) the luminescence burst, respectively. The raw data for the spectra of the PL and reflected laser light is presented in Figure S6, Supporting Information. By referring to the blue dashed line, which shows the linear dependence of the reflected laser light intensity on the excitation irradiance when only the linear absorption is present, we were able to derive the nonlinear absorption (N_2^{abs}). It is noticed that the PL (N_2^{pl}) of the Ga/Ga_2O_3 NP is stronger than that of the Ga NP while the corresponding nonlinear absorption (N_2^{abs}) of the former is smaller than the latter by one order magnitude. In Figure 3e, we present the quantum efficiencies derived for the Ga and Ga/Ga_2O_3 NPs at different excitation irradiances. It can be seen that the quantum efficiency of Ga/Ga_2O_3 NPs (≈1.3%) is nearly two orders of magnitude larger than that of Ga NPs (≈4.5 × 10^{-4}). Owing to the photo-thermal effect and Auger recombination, the quantum efficiency of Ga/Ga_2O_3 NPs decreases gradually with increasing irradiance (Figure S7, Supporting Information). For comparison, we also performed PL measurements for Ga_2O_3 microparticles. Considering that Ga_2O_3 microparticles have neither resonances nor plasmonic hotspots, the PL from Ga_2O_3 microparticles is very weak even at a large excitation irradiance (6 mJ cm^{-2}) (Figure S8, Supporting Information).

In order to achieve a large local field enhancement, we fabricated closely-packed Ga nanoislands with plasmonic hotspots in between them by using a thermal evaporation system, as shown in the inset of **Figure 4**a (Figure S9, Supporting Information). Based on the SEM image, we established a physical model for closely-packed Ga nanoislands and simulated the electric field distribution by using the finite-difference

© 2021 Wiley-VCH GmbH

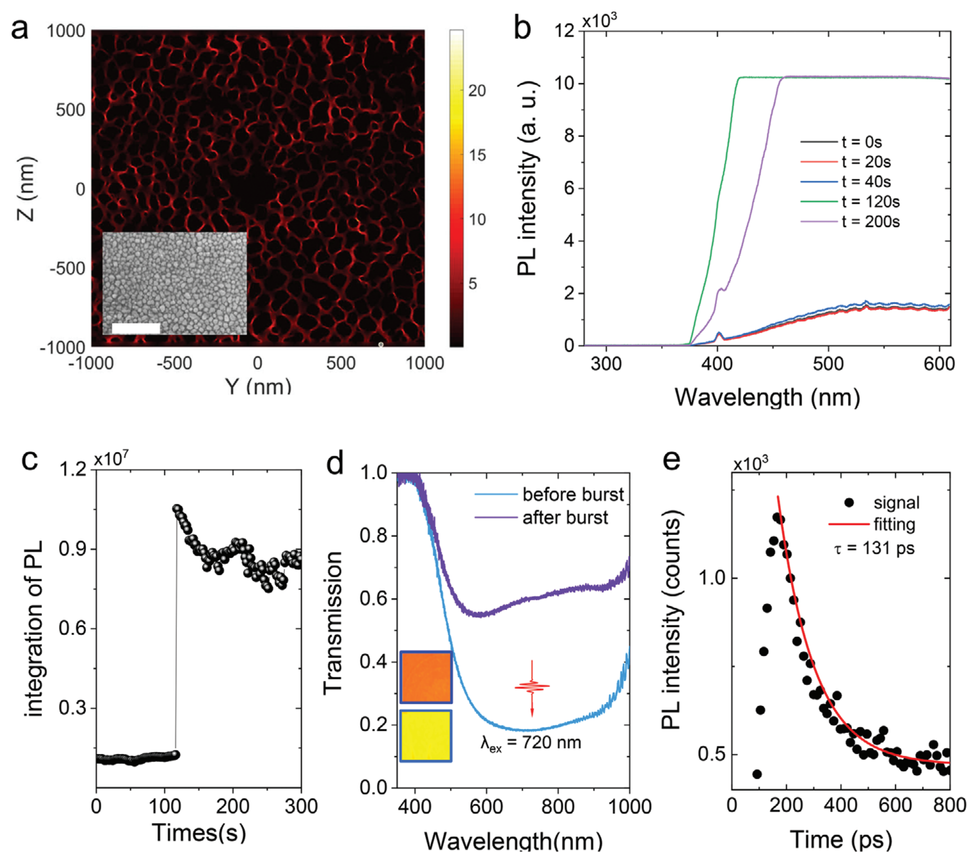

Figure 4. Hot-electron luminescence from closely-packed Ga nanoislands. a) Electric field distribution calculated for closely-packed Ga nanosialnds at $\lambda = 720$ nm. The morphology of closely-packed Ga nanoislands characterized by SEM is shown in the inset. b) PL spectra of closely-packed Ga nanoislands measured at different excitation times. Here, the excitation irradiance was fixed at 2.0 mJ cm^{-2}. c) Dependence of the integrated PL intensity of Ga nanoislands on the irradiation time. d) Transmission spectra measured for closely-packed Ga nanoislands before and after the laser irradiation. The bright-field images of the Ga nanoislands recorded by using a CCD are shown in the insets. e) Luminescence decay measured for the Ga nanoislands.

time-domain technique. Figure 4a shows the electric-field distribution obtained at a wavelength of 720 nm. One can see many plasmonic hotspots in the gap regions between Ga nanoislands, which localize the electric field with an enhancement factor of ≈25. These hotspots can significantly enhance the absorption cross-section and reduce the threshold for luminescence burst. It is remarkable that these hotspots create a broadband optical response, which is confirmed by the transmission spectrum. Since Ga nanoislands can be excited more effectively by using laser light with a larger photon energy, we employed femtosecond laser pulses at 720 nm to examine the luminescence burst of Ga nanoislands. The femstosecond laser light was focused on Ga nanoislands with a fixed irradiance of 2.0 mJ cm^{-2} and the PL spectrum was measured repeatedly with a time interval of 2.0 s. Figure 4b shows the typical PL spectra obtained at different times. Unlike the PL spectra of Ga NPs discussed above, we presented only the PL spectra below 610 nm because a high-pass filter was used in the measurements. It is noticed that the PL intensity was increased by one order of magnitude after the burst and it exceeded the detection limit of the CCD. The evolution of the integrated PL intensity with increasing time (t) is shown in Figure 4c. For $t < 115$ s, the PL intensity remained nearly unchanged. At $t = 115$ s, a rapid increase in the PL intensity was observed, indicating the transition from Ga nanoislands to Ga/Ga_2O_3 ones. To gain a deep insight into such as the transition induced by femtosecond laser pulses, we measured the transmission spectra of Ga nanoislands before and after the luminescence burst, as shown in Figure 4d. The corresponding bright-field images of Ga nanoislands recorded by using the CCD are shown in the insets. Remarkably, an enhanced transmission was observed after the luminescence burst due to the formation of Ga/Ga_2O_3 nanoislands. We also measured the luminescence lifetime of the Ga/Ga_2O_3 nanoislands, as shown in Figure 4e. The lifetime derived from the luminescence decay was found to be ≈130 ps, which is much longer than that of Ga nanoislands (<10 ps).[23] It indicates that the transfer of hot electrons from Ga_2O_3 to Ga in the Ga/Ga_2O_3 nanoislands leads to a longer luminescence lifetime. The enhanced transmission in combination with the prolonged lifetime strongly support the laser-induced oxidation model proposed in this work.

The existence of randomly distributed hotspots induced by the plasmonic coupling between Ga nanoislands can be exploited to realize optical memory with ultralow energy and ultrahigh density.[41,42] As a proof-of-principle demonstration, we employed closely-packed Ga nanoislands to implement optical data storage. First, we demonstrated data recording and readout by using a laser scanning confocal microscope

© 2021 Wiley-VCH GmbH

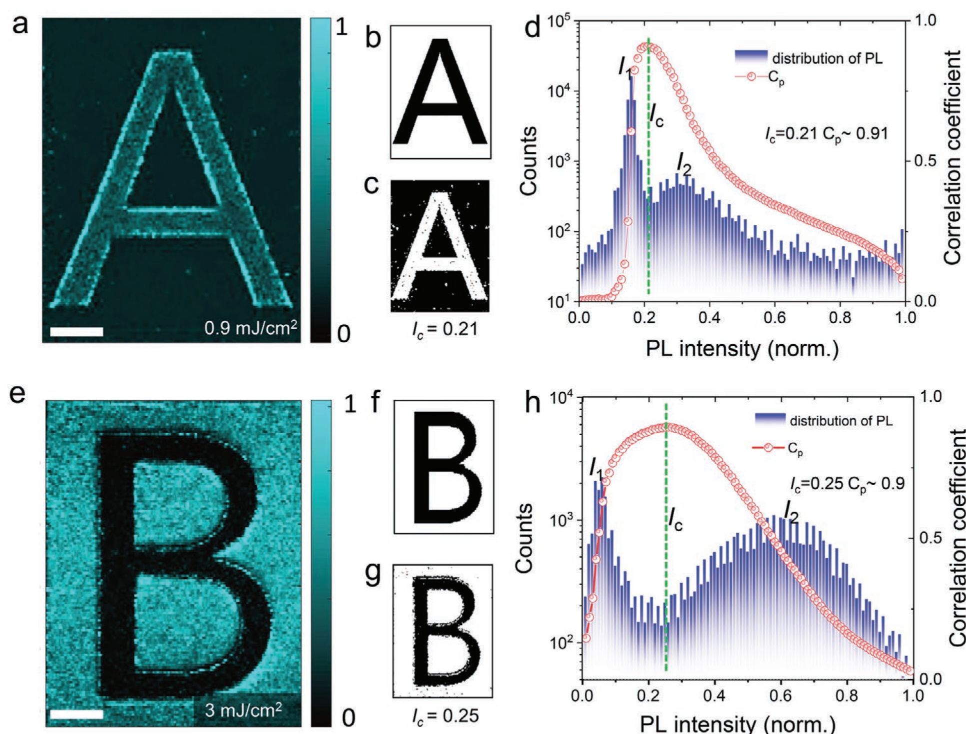

Figure 5. Optical data storage realized by in closely-packed Ga nanoislands. a) Pattern recorded and extracted in closely-packed Ga nanoislands by using 800-nm femtosecond laser pulses with relatively small irradiances of 0.9 (below the burst threshold) and 0.3 mJ cm^{-2}. b) Original pattern used for data recording and readout. c) Binary pattern extracted from the PL pattern shown in (a) with a threshold of $I_c = 0.21$. d) Distribution of the PL intensities of all the pixels and the dependence of the correlation coefficient on the threshold intensity. e) Pattern recorded and extracted in closely-packed Ga nanoislands by using 800-nm femtosecond laser pulses with relatively small irradiances of 3.0 (above the burst threshold) and 0.5 mJ cm^{-2}. f) Original pattern used for data recording and readout. g) Binary pattern extracted from the PL pattern shown in (e) with a threshold of $I_c = 0.25$. h) Distribution of the PL intensities of all the pixels and the dependence of the correlation coefficient on the threshold intensity. The length of the scale bars in (a,e) is 20 µm.

with a small irradiance (below the burst threshold), as shown in **Figure 5**a–d. Figure 5a shows the extracted pattern, which is a letter "A", recorded in Ga nanoislands by using 800-nm femtosecond laser pulses with the recording and readout irradiances of 0.9 and 0.3 mJ cm^{-2}, respectively. The original pattern is shown in Figure 5b where the white region represents the laser scanning area. During the recording process, the plasmonic hotspots in Ga nanoislands were wiped by the laser light (0.9 mJ cm^{-2}) and the PL of the laser-irradiated area will extinguish during the readout process (0.3 mJ cm^{-2}). To characterize the quality (or error rate) of the extracted pattern, we used the Pearson correlation coefficient (C_p), which is defined as follows, to measure the degree of linear correlation between the original and extracted patterns.

$$C_p = \sum_m \sum_n \left(X_{mn} - \bar{X}\right)\left(Y_{mn} - \bar{Y}\right) / \sqrt{\sum_m \sum_n \left(X_{mn} - \bar{X}\right)^2 \left(Y_{mn} - \bar{Y}\right)^2} \tag{2}$$

Here, X_{mn} and Y_{mn} represent the intensities of the individual pixels (m, n) while X and Y denote the averaged intensities of all the pixels in the original and extracted patterns, respectively. Figure 5c shows the extracted binary pattern when the threshold intensity (I_c) was set at 0.21, where the largest correlation coefficient is achieved ($C_p \approx 0.91$). It is noticed that the original and recovered patterns in this case are complementary. It implies that the PL intensity of the Ga nanoislands was reduced by laser irradiation when the excitation irradiance is below the burst threshold, similar to phenomenon observed previously.[41–43] From the extracted pattern shown in Figure 5a, we obtained the distribution of the PL intensities of all the pixels, as shown in Figure 5d. The dependence of C_p on I_c is also presented. As demonstrated above, laser-induced oxidation occurs for Ga nanoislands when the excitation irradiance exceeds the threshold, leading to a significant increase in the PL intensity. This unique feature can also be employed to realize optical memory in a similar way. In Figure 5e, we show the extracted pattern, which is a letter "B", recorded in Ga nanoislands with the recording and readout irradiances of 3.0 (above burst threshold) and 0.5 mJ cm^{-2}, respectively. The original pattern is shown Figure 5f where the white region demotes the laser scanning area. In this case, the extracted pattern agrees with the original one, indicating the enhanced PL intensity induced by laser irradiation. Similarly, high-quality data storage with $C_p \approx 0.90$ was achieved when the I_c was set at 0.25, as shown in Figure 5h.

3. Conclusion

In conclusion, we proposed and demonstrated efficient white light emitters and high-quality optical data storage based on

© 2021 Wiley-VCH GmbH

liquid Ga NPs and nanoislands. It was found that Ga/Ga_2O_3 NPs can be obtained by using laser-induced oxidation, which breaks the self-terminating oxidation of Ga NPs. Owing to the enhanced multiphoton-induced absorption in Ga/Ga_2O_3 and effective electron transfer at the Ga-Ga_2O_3 junction, a luminescence burst was observed when the excitation irradiance exceeds a threshold. The quantum efficiency for the PL of Ga/Ga_2O_3 NPs was found to be ≈1.3%, which is enhanced by two orders of magnitude as compared with the value of Ga NPs. The broadband PL from Ga/Ga_2O_3 NPs was identified as hot-electron intraband luminescence. As an example of practical applications, we demonstrated high-quality optical data storage by exploiting the laser-induced oxidation of Ga nanoislands. The efficient white light emission from Ga/Ga_2O_3 NPs makes them a promising candidate for nanoscale broadband light source with a wide range of applications in nanospectroscopy and bioimaging. Moreover, the optical data storage demonstrated in closely-packed Ga nanoislands may facilitate the development of data storage in flexible electronics and wearable biometric devices.

4. Experimental Section

Experimental Details: Ga NPs with diameters ranging from 50 to 300 nm where fabricated by using femtosecond laser ablation of a Ga film immersed in water. A femtosecond laser amplifier (Legend, Coherent) with a pulse duration of 100 fs and a repetition rate of 1 kHz was employed in the ablation process. An objective with 25-cm focal length was used to focus the femtosecond laser beam on the Ga film with a spot diameter of ≈40 mm. Ga NPs ejected from the Ga film after the irradiation of femtosecond laser light were uniformly dispersed in water. For optical characterization, they were randomly distributed on a thin Au film. The backward scattering spectra of Ga NPs were measured by using a long working distance objective (Nikon, Plan SLWD, 50×, NA = 0.4) with an external white light source for illumination (see Figure S1, Supporting Information). The incident light can be either s- or p-polarized by using a polarizer. The characterization of the nonlinear optical properties of Ga NPs was carried out by using a femtosecond laser oscillator (Mira-900S, Coherent) with pulse duration of 130 fs and a repetition rate of 76 MHz. The femtosecond laser light was introduced into an inverted microscope and focused on Ga NPs by using a 100× objective. The nonlinear optical signals from Ga NPs were collected by the same objective and directed to a spectrometer (SR500, Andor) for analysis.

Data recording and readout were completed by using the laser scanning confocal microscope (A1MP, Nikon). The femtosecond laser light with a repetition rate of 76 MHz and a duration of 130 fs (Mira 900S, Coherent) was employed for optical data storage in closely-packed Ga nanoislands. It was focused on the samples by using the 60× objective lens (NA = 0.85) of a two-photon confocal laser scanning confocal microscope (A1MP, Nikon). The PL in the wavelength range of 450–650 nm was detected.

Numerical Modeling: The electric field distribution in closely-packed Ga nanoislands was calculated by using the finite-difference time domain (FDTD) technique. In the FDTD simulation, the smallest non-uniform mesh size of 1 nm as well as a perfectly matched boundary condition was employed. The complex refractive indices for liquid Ga used in the numerical simulations were taken from literature.[23]

Supporting Information

Supporting Information is available from the Wiley Online Library or from the author.

Acknowledgements

The authors acknowledge the financial support from the National Natural Science Foundation of China (Grant Nos. 11874020 and 61975072), the Science and Technology Program of Guangzhou (No. 2019050001), the Program for Innovative Research Team in Science and Technology in Fujian Province University (No. 2020H6017), the Scientific Research Foundation of the Education Department of Fujian Province (No. JT180296), the Natural Science Foundation of Zhangzhou (ZZ2021J11), and the Scientific Research Project of Minnan Normal University (Nos. MX1601 and KJ19020). The authors would like to thank Mr. Michael Bergmann for his help in English polishing.

Conflict of Interest

The authors declare no conflict of interest.

Data Availability Statement

Research data are not shared.

Keywords

Ga nanoparticles, laser-induced oxidation, liquid metal, metal–semiconductor junction, optical memory

Received: April 3, 2021
Revised: July 9, 2021
Published online:

[1] Z. Fang, X. Zhu, *Adv. Mater.* **2013**, *25*, 3840.
[2] J. N. Anker, W. P. Hall, O. Lyandres, N. C. Shah, J. Zhao, R. P. Van Duyne, *Nat. Mater.* **2008**, *7*, 442.
[3] E. C. Dreaden, A. M. Alkilany, X. Huang, C. J. Murphy, M. A. El-Sayed, *Chem. Soc. Rev.* **2012**, *41*, 2740.
[4] P. Zijlstra, M. Orrit, *Rep. Prog. Phys.* **2011**, *74*, 106401.
[5] T. Daeneke, K. Khoshmanesh, N. Mahmood, I. A. de Castro, D. Esrafilzadeh, S. J. Barrow, M. D. Dickey, K. Kalantar-zadeh, *Chem. Soc. Rev.* **2018**, *47*, 4073.
[6] J. M. Mcmahon, G. C. Schatz, S. K. Gray, *Phys. Chem. Chem. Phys.* **2013**, *15*, 5415.
[7] C. Yi, T.-H. Kim, W. Jiao, Y. Yang, A. Lazarides, K. Hingerl, G. Bruno, A. Brown, M. Losurdo, *Small* **2012**, *8*, 2721.
[8] S. Kim, J.-M. Kim, J.-E. Park, J.-M. Nam, *Adv. Mater.* **2018**, *30*, 1704528.
[9] P. C. Wu, C. G. Khoury, T.-H. Kim, Y. Yang, M. Losurdo, G. V. Bianco, T. Vo-Dinh, A. S. Brown, H. O. Everitt, *J. Am. Chem. Soc.* **2009**, *131*, 12032.
[10] P. C. Wu, M. Losurdo, T.-H. Kim, M. Giangregorio, G. Bruno, H. O. Everitt, A. S. Brown, *Langmuir* **2009**, *25*, 924.
[11] Y. Yang, J. M. Callahan, T.-H. Kim, A. S. Brown, H. O. Everitt, *Nano Lett.* **2013**, *13*, 2837.
[12] P. Albella, B. Garcia-Cueto, F. Gonzalez, F. Moreno, P. C. Wu, T.-H. Kim, A. Brown, Y. Yang, H. O. Everitt, G. Videen, *Nano Lett.* **2011**, *11*, 3531.
[13] B. F. Soares, F. Jonsson, N. I. Zheludev, *Phys. Rev. Lett.* **2007**, *98*, 153905.
[14] K. F. MacDonald, V. A. Fedotov, N. I. Zheludev, *Appl. Phys. Lett.* **2003**, *82*, 1087.

 © 2021 Wiley-VCH GmbH

[15] W. T. Liang, L. Hong, H. Yang, F. F. Fan, Y. Liu, H. Li, J. Li, J. Y. Huang, L. Q. Chen, T. Zhu, S. L. Zhang, *Nano Lett.* **2013**, *13*, 5212.
[16] M. Losurdo, A. Suvorova, S. Rubanov, K. Hingerl, A. S. Brown, *Nat. Mater.* **2016**, *15*, 995.
[17] K. Kalantar-Zadeh, J. B. Tang, T. Daeneke, A. P. O'Mullane, L. A. Stewart, J. Liu, C. Majidi, R. S. Ruoff, P. S. Weiss, M. D. Dickey, *ACS Nano* **2019**, *13*, 7388.
[18] S. V. Makarov, I. S. Sinev, V. A. Milichko, F. E. Komissarenko, D. A. Zuev, E. V. Ushakova, I. S. Mukhin, Y. F. Yu, A. I. Kuznetsov, P. A. Belov, I. V. Iorsh, A. N. Poddubny, A. K. Samusev, Y. S. Kivshar, *Nano Lett.* **2018**, *18*, 535.
[19] F. Lu, M. Jin, M. A. Belkin, *Nat. Photonics* **2014**, *8*, 307.
[20] S. Viarbitskaya, A. Teulle, R. Marty, J. Sharma, C. Girard, A. Arbouet, E. Dujardin, *Nat. Mater.* **2013**, *12*, 426.
[21] P. Ghenuche, S. Cherukulappurath, T. H. Taminiau, N. F. van Hulst, R. Quidant, *Phys. Rev. Lett.* **2008**, *101*, 116805.
[22] J. Xiang, S. Jiang, J. Chen, J. Li, Q. Dai, C. Zhang, Y. Xu, S. Tie, S. Lan, *Nano Lett.* **2017**, *17*, 4853.
[23] J. Xiang, J. D. Chen, S. Jiang, M. C. Panmai, P. L. Li, Y. Xu, Q. F. Dai, S. L. Tie, S. Lan, *Laser Photonics Rev.* **2019**, *13*, 1800214.
[24] T. Haug, P. Klemm, S. Bange, J. M. Lupton, *Phys. Rev. Lett.* **2015**, *115*, 067403.
[25] E. Dulkeith, T. Niedereichholz, T. A. Klar, J. Feldmann, G. von Plessen, D. I. Gittins, K. S. Mayya, F. Caruso, *Phys. Rev. B* **2004**, *70*, 205424.
[26] J. Xiang, J. D. Chen, Q. F. Dai, S. L. Tie, S. Lan, A. E. Miroshnichenko, *Phys. Rev. Appl.* **2020**, *13*, 014003.
[27] C. Zhang, Y. Xu, J. Liu, J. Li, J. Xiang, H. Li, J. Li, Q. Dai, S. Lan, A. E. Miroshnichenko, *Nat. Commun.* **2018**, *9*, 2964.
[28] J. Xiang, M. Panmai, S. Bai, Y. Ren, G.-C. Li, S. Li, J. Liu, J. Li, M. Zeng, J. She, Y. Xu, S. Lan, *Nano Lett.* **2021**, *21*, 2397.
[29] E. Xifre-Perez, L. Shi, U. Tuzer, R. Fenollosa, F. Ramiro-Manzano, R. Quidant, F. Meseguer, *ACS Nano* **2013**, *7*, 664.
[30] I. Sinev, I. Iorsh, A. Bogdanov, D. Permyakov, F. Komissarenko, I. Mukhin, A. Samusev, V. Valuckas, A. I. Kuznetsov, B. S. Luk'yanchuk, A. E. Miroshnichenko, Y. S. Kivshar, *Laser Photonics Rev.* **2016**, *10*, 799.
[31] C. Lumdee, B. Yun, P. G. Kik, *ACS Photonics* **2014**, *1*, 1224.
[32] D. Y. Lei, A. I. Fernandez-Dominguez, Y. Sonnefraud, K. Appavoo, R. F. HaglundJr., J. B. Pendry, S. A. Maier, *ACS Nano* **2012**, *6*, 1380.
[33] A. E. Miroshnichenko, S. Flach, Y. S. Kivshar, *Rev. Mod. Phys.* **2010**, *82*, 2257.
[34] B. Luk'yanchuk, N. I. Zheludev, S. A. Maier, N. J. Halas, P. Nordlander, H. Giessen, C. T. Chong, *Nat. Mater.* **2010**, *9*, 707.
[35] H. D. Deng, G. C. Li, Q. F. Dai, M. Ouyang, S. Lan, V. A. Trofimov, T. M. Lysak, *Nanotechnology* **2013**, *24*, 075201.
[36] M. W. Knight, T. Coenen, Y. Yang, B. J. M. Brenny, M. Losurdo, A. S. Brown, H. O. Everitt, A. Polman, *ACS Nano* **2015**, *9*, 2049.
[37] L. Nanai, R. Vajtai, T. F. George, *Thin Solid Films* **1997**, *298*, 160.
[38] X. F. Li, C. Y. Zhang, H. Li, Q. F. Dai, S. Lan, S. L. Tie, *Opt. Express* **2014**, *22*, 28086.
[39] F. Herziger, R. Mirzayev, E. Poliani, J. Maultzsch, *Phys. Status Solidi B* **2015**, *252*, 2451.
[40] C. J. Powell, *Phys. Rev.* **1968**, *175*, 972.
[41] Q. Dai, M. Ouyang, W. Yuan, J. Li, B. Guo, S. Lan, S. Liu, Q. Zhang, G. Lu, S. Tie, H. Deng, Y. Xu, M. Gu, *Adv. Mater.* **2017**, *29*, 1701918.
[42] M. C. Xian, Y. Xu, X. Ouyang, Y. Y. Cao, S. Lan, X. P. Li, *Sci. Bull.* **2020**, *65*, 2072.
[43] P. Zijlstra, J. W. M. Chon, M. Gu, *Nature* **2009**, *459*, 410.

© 2021 Wiley-VCH GmbH